NANO LETTERS

pubs.acs.org/NanoLett Letter

Probing Single-Particle Electrocatalytic Activity at Facet-Controlled Gold Nanocrystals

Myunghoon Choi,[‡] Natasha P. Siepser,[‡] Soojin Jeong,[‡] Yi Wang, Gargi Jagdale, Xingchen Ye,* and Lane A. Baker*

Cite This: *Nano Lett.* 2020, 20, 1233−1239 Read Online

ACCESS | Metrics & More | Article Recommendations | Supporting Information

ABSTRACT: Electrocatalytic reduction reactions (i.e., the hydrogen evolution reaction (HER) and oxygen reduction reaction) at individual, faceted Au nanocubes (NCs) and nano-octahedra (ODs) expressing predominantly {100} and {111} crystal planes on the surface, respectively, were studied by nanoscale voltammetric mapping. Cyclic voltammograms were collected at individual nanoparticles (NPs) with scanning electrochemical cell microscopy (SECCM) and correlated with particle morphology imaged by electron microscopy. Nanoscale measurements from a statistically informative set of individual NPs revealed that Au NCs have superior HER electrocatalytic activity compared to that of Au ODs, in good agreement with macroscale cyclic voltammetry measurements. Au NCs exhibited more particle-to-particle variation in catalytic activity compared to that with Au ODs. The approach of single-particle SECCM imaging coupled with macroscale CV on well-defined NPs provides a powerful toolset for the design and activity assessment of nanoscale electrocatalysts.

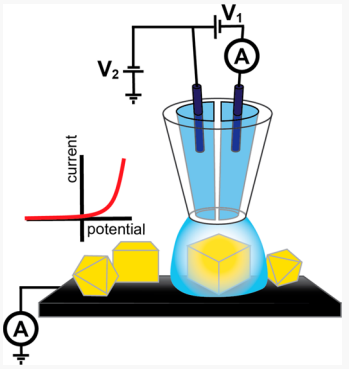

KEYWORDS: *scanning electrochemical cell microscopy, SECCM, nanocubes, nano-octahedra, single-particle catalysis, facet-dependent catalytic activity*

Synthetic control of surface faceting is a versatile and effective method to tailor the electrocatalytic activity of nanoparticle (NP) catalysts.[1−3] The preferential exposure of high-energy facets on NP surfaces can help lower the required energy barrier for a reaction by altering the adsorption energy and desorption rate of critical reaction intermediates associated with rate-limiting steps.[4] Furthermore, control of NP surface termination can aid in the enhancement of the electrochemical reaction selectivity by suppressing competing reaction pathways or byproduct interference, which may decrease catalytic activity.[5]

Quantification of facet-dependent catalytic activity of NPs is essential to establishing guidelines for the rational design of NP electrocatalysts. However, sample heterogeneity stemming from variations in particle size and morphology, the presence of surface ligands,[6] and limitations in methodological approaches often make it difficult to understand the facet-dependent electrocatalytic activity.[7−9] Macroscopic voltammetric techniques, such as cyclic voltammetry (CV), are generally used to study NP catalyst ensembles to deduce the averaged properties of a catalyst sample. Interpretation of macroscale electrochemical measurement results can be complicated due to the presence of NP aggregates or variable surface coverage of NPs on the electrode surface. Even when such inhomogeneities in NP deposition are minimized, the challenge in accurate assessment of facet-dependent activity and selectivity still remains because current state-of-the-art synthetic methods do not produce atomically precise NPs.

Over the past decade, single-particle electrochemical measurements have gained popularity as a means to study the catalytic property of individual NPs and to establish how individual NPs contribute to the macroscale (ensemble) measurements.[10−12] Scanning electrochemical cell microscopy (SECCM) is a scanning droplet technique in which a droplet at the tip of a submicrometer pipet contacts a semiconductive surface and spatially maps the electrochemical activity.[11−15] Introduction of this technique by Unwin and co-workers has opened a new era in nanoscale electrochemical imaging. With SECCM and its variants such as scanning micropipet contact microscopy[16,17] and optically targeted electrochemical cell microscopy,[18] a range of electrochemical measurements including cyclic voltammetry,[19] linear sweep voltammetry,[20] and galvanostatic measurements[21] can now be conducted at well-defined positions with high spatial resolution and low background capacitance. More recent developments of the voltammetric hopping mode[19] and coupling of SECCM with other spectroscopic techniques in a "correlative multi-microscopy approach" have further expanded the versatility of the SECCM technique and allowed for the unequivocal

Received: November 11, 2019
Revised: December 27, 2019
Published: January 9, 2020

https://dx.doi.org/10.1021/acs.nanolett.9b04640
Nano Lett. 2020, 20, 1233−1239

correlation between nanoscale sample morphology and catalytic performance.[12] In the voltammetric hopping mode, a droplet contacts the sample at a series of predefined locations. At each location, the potential is swept at the substrate and the electrochemical current is measured. SECCM has probed the electrocatalytic activity of individual NPs, such as iridium oxide particles for water splitting,[22] Pt NPs electrodeposited on single-walled carbon nanotubes[23] and Pt nanoclusters[24] for the oxygen reduction reaction (ORR), Au nanorods[18] and electrodeposited Au NPs for hydrazine electrooxidation,[25] and Au(111) nanoclusters,[26] hexagonal boron nitride sheets,[20] doped holey graphene,[27] and dichalcogenide nanosheets[28] for the hydrogen evolution reaction (HER), and single ZIF-derived nanocomposite particles for the oxygen evolution reaction (OER).[29] To the best of our knowledge, SECCM has not yet been used to elucidate facet-dependent electrocatalysis at the single-particle level from a heterogeneous ensemble of NP catalysts.

In this work, we studied reduction reactions (HER and ORR) on model Au NP catalysts with well-defined surface facets with SECCM CV mapping. A dual barrel nanopipet (outer diameter ~200 nm) was utilized as the SECCM probe to define the droplet cell dimensions to study single Au NPs with edge lengths of <100 nm (scale drawing, Figure S1). Here SECCM was performed on a modified commercial microscope (Park Systems, South Korea) which combined a nanoscale probe positioning system and custom two-electrode potentiostat (Figure 1a). The SECCM probe was engaged with the substrate, which serves as the working electrode (WE), by alternating current (AC) mode[14,15] feedback to prevent physical contact with or probe-end damage by the WE and to hold the pipet position during CV acquisition. An AC current (<50 pA) across the droplet was generated by applying a constant potential (V_1) between the Ag/AgCl quasi-reference counter electrodes inserted into each barrel of the pipet and modulating the pipet's vertical position (~10 nm). In conjunction with AC feedback control for each droplet−substrate contact event, hopping mode[30,31] (also called approach−retract scanning mode)[32] was used. After droplet−substrate contact, the potential (V_2) was swept and the current was measured at the substrate to collect a CV. A SECCM CV map was constructed by recording the CV response at several locations (pixels) over a predefined area.

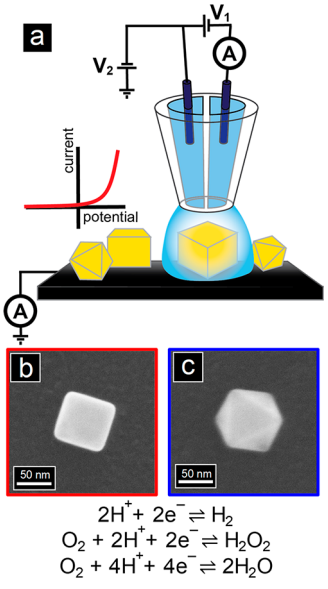

Figure 1. (a) Schematic of SECCM CV mapping at individual, faceted Au nanocrystals for the HER/ORR. A potential, V_1, is applied to generate an ion current between the two Ag/AgCl electrodes in each barrel of the pipet. A potential, V_2, is swept to collect a cyclic voltammogram, and the substrate current is measured. High-resolution electron micrograph of (b) a single Au nanocube (Au NC) and (c) a single Au nano-octahedra (OD).

A statistically meaningful set of single-particle measurements was collected at Au NCs, Au ODs, as well as their physical mixtures to determine the facet-dependent electrocatalytic response. Au NCs and ODs with narrow size distributions and nearly identical surface areas (sum of five {100} NC faces equals seven {111} OD faces) were synthesized, so that any difference in electrocatalytic responses can be attributed to the exposed surface facet (Figures S2 and S3 and Table S1). Scanning electron microscopy (SEM) images of individual Au NC (edge length of ~78 nm) and OD (edge length of ~99 nm) illustrate the well-faceted nature of these NPs (Figure 1b,c). Electrodes were prepared by drop-casting NPs onto polished glassy carbon substrates (Figures S4 and S5). We utilized a two-step protocol to remove excess cetyltrimethylammonium bromide (CTAB) on the Au NPs so that their intrinsic electrocatalytic properties could be studied. First, glassy carbon substrates coated with Au NPs were immersed in methanol for approximately 2 min to remove the majority of CTAB ligands. The duration of methanol treatment was optimized by monitoring the intensity of the C−H stretching vibrations with Fourier transform infrared (FTIR) spectroscopy (Figure S6). Next, deposited NP catalysts were cleaned by CV cycling.[33] The disappearance of insulating ligand "halos" coating the as-synthesized Au NPs was monitored by using SEM at different stages of ligand stripping (Figures S7 and S8). Based on SEM imaging results, removal of CTAB ligands from Au ODs appeared to be more difficult than removing them from Au NCs, suggesting that CTAB may bind more strongly to Au{111} than to Au{100} surfaces. Recent molecular dynamics (MD) simulations have predicted that the surface density of CTAB at Au{111} surfaces was higher than that at {100} surfaces in the presence of Cl^-.[34] This theoretical prediction is in line with our experimental results considering that cetylpyridinium chloride (CPC) was used during synthesis of Au NC and OD.

Macroscale linear sweep voltammogram (LSV) measurements were performed to compare the HER activity between Au NCs and ODs. All macroscale measurements were carried out in a custom-made three-electrode cell and corrected for IR drop (Figures S10 and S11). To correlate macroscale measurement with single-particle SECCM results, glassy carbon substrates sparsely covered with the same amount of Au NCs and ODs were examined (Figure 2a,b and section S3.4). Au NCs reached a current density of 1 mA/cm^2 (normalized by the geometric area of glassy carbon electrode) at ~30 mV more positive potential than with Au ODs, suggesting more favorable kinetics for NCs than ODs (Figure 2c). Our results agree with previous experiments carried out on Au single crystals by Weaver and co-workers,[35] although earlier investigations on the HER at single-crystal Au electrodes revealed a minor dependence on crystallographic termination.[35−38] The electrocatalytic current at the faceted Au NPs began to increase at approximately −0.7 vs Ag/AgCl, which was consistent with previous scanning electrochemical

https://dx.doi.org/10.1021/acs.nanolett.9b04640
Nano Lett. 2020, 20, 1233−1239

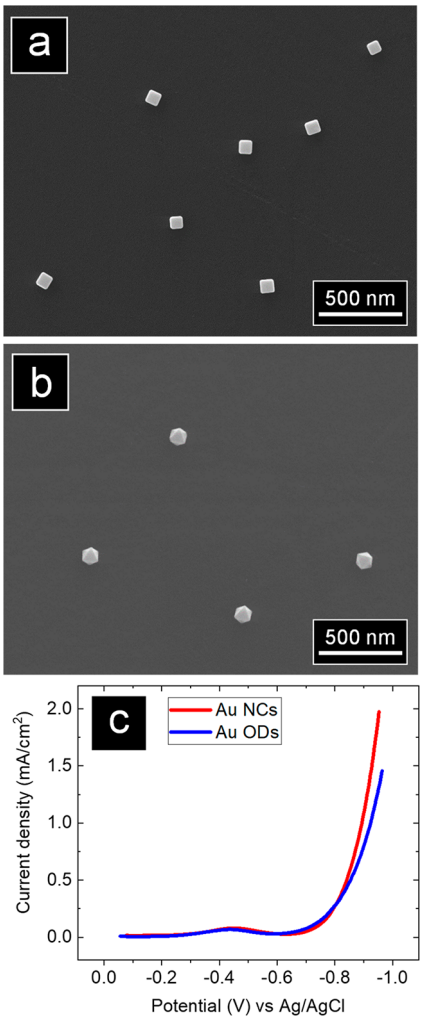

Figure 2. Representative electron micrographs of (a) Au NCs and (b) Au ODs utilized for (c) macroscale LSVs (aqueous 100 mM $HClO_4$, scan rate = 50 mV/s).

microscopy (SECM) results from the Mirkin group, in which a single Au NP was attached to a carbon nanoelectrode through a multilayer polyphenylene linker.[39] We postulate that CTAB ligands were still present at the interface between the bottom flat facet of the Au NC or OD and the glassy carbon electrode, which could impede efficient electron transfer and result in higher overpotentials. LSV experiments conducted in N_2-, air-, and O_2-purged electrolyte solution revealed that the peak around −0.45 V vs Ag/AgCl can be attributed to the ORR catalyzed by Au NPs, and that HER was the predominant reaction that took place at potentials more negative than approximately −0.6 V vs Ag/AgCl (Figure S12).

To better understand the HER activity at the single-particle level, Au NC and OD samples were studied separately by SECCM. All SECCM voltammetric data were reported with respect to a Ag/AgCl (3.5 M NaCl) reference electrode. Figure 3a shows the SECCM CV map at −0.95 V vs Ag/AgCl for Au NCs. This potential was chosen to highlight the difference in current magnitude between Au NPs and the underlying glassy carbon substrate. At each pixel in the CV map, the potential at the Au NP sample was swept from −0.4 to −0.95 V vs Ag/AgCl at a scan rate of 1 V/s. Pixels corresponding to Au NPs showed a higher current signal than the background substrate current, as confirmed by correlative SECCM and SEM imaging (section S5 and Figures S20 and S21). Enhanced current signal at 1−3 pixels were observed for isolated Au NPs. Single Au NPs represented by more than one pixel are attributed to multiple instances of droplet contact to the same Au NP. For example, the pixel outlined by the green circle in Figure 3a corresponds to a single Au NC (Figure 3b−d), for which the background-subtracted CV scan (Figure 3c) is also included. Details regarding the background subtraction for CVs collected by SECCM are presented in Figure S19. A SECCM CV map of Au ODs acquired at the same potential of −0.95 V vs Ag/AgCl, the corresponding SEM image of the sample area studied, and the background-subtracted CV response for a single Au OD are depicted in Figure 3e−h. The number of pixels corresponding to isolated Au ODs varied between 1 and 2 pixels. Importantly, the current level measured from individual Au ODs was significantly smaller than that of single Au NCs at the same potential (−0.95 V vs Ag/AgCl). The SECCM CV data for 70 individual Au NCs and 64 individual Au ODs, corresponding to 101 and 99 pixels, respectively, were then averaged. The average current response included all pixels from individual Au NCs and ODs. Clusters of multiple NPs were excluded in these calculations. In Figure 3i, the averaged CV result exhibited a clear difference in the current magnitude between Au NCs and ODs at potentials more negative than approximately −0.75 V. The distribution of current responses at −0.75, −0.85, and −0.95 V vs Ag/AgCl for 101 pixels of Au NCs and 99 pixels of Au ODs are summarized and presented as histograms in Figure 3j. Au ODs exhibited a narrower distribution in current magnitudes compared to that with Au NCs. The average currents and 99.9% confidence intervals for Au NCs and Au ODs at −0.95 V vs Ag/AgCl were 170 ± 20 and 70 ± 10 pA, respectively, and were determined to be statistically different (Figure 3j). Differences in electrocatalytic response observed with single-particle SECCM measurements suggest more favorable HER kinetics on the surface of NCs than ODs. Importantly, measurements of the same nanoparticle in consecutive images (3−5) were highly reproducible (within several picoamperes at the maximum current).

Our single-particle SECCM measurements (Figure 3i) showed a similar trend to macroscale CV experiments (Figure 2c), where Au NCs showed higher HER activity compared to that with ODs. Previous density functional theory calculations also suggested that Au(100) can be a superior catalyst for the HER compared to Au(111) because Au(100) exhibited a more negative hydrogen adsorption energy favoring hydrogen adsorption.[40] Although a direct comparison between macroscale and SECCM experimental results is difficult as the former reports a convolution in response from single particles, clusters, and misshaped particles, the maximum potential difference between the Au NCs and Au ODs was ∼100 and 50 mV from SECCM and macroscale studies, respectively. A unique advantage of correlative SECCM with electron microscopy, over macroscale electrochemical measurements, is the electrochemical responses at clusters and misshaped particles can be identified and separated from the responses for the correctly faceted individual particles. As a result, the average CV response by SECCM is for a set of individual particles with minimal heterogeneity in size and shape, which is challenging to achieve on a macroscale electrode with common sample preparation techniques.

To further clarify the differences between particle types under identical conditions, we conducted SECCM experiments

https://dx.doi.org/10.1021/acs.nanolett.9b04640
Nano Lett. 2020, 20, 1233−1239

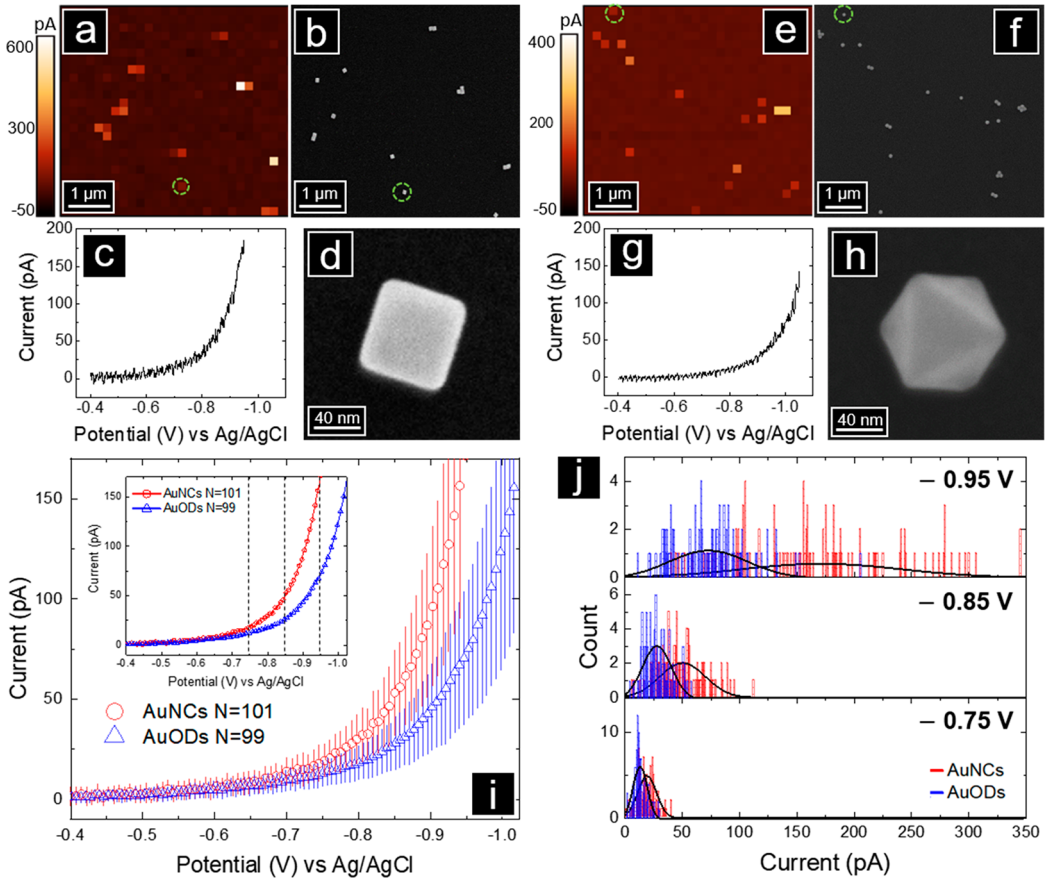

Figure 3. (a) Au NC SECCM CV map at −0.95 V vs Ag/AgCl, (b) correlative electron micrograph of SECCM area, (c) respective CV for the single particle (highlighted by green dashed circle), and (d) high-resolution electron micrograph. (e) Au OD SECCM CV map at −1.05 V vs Ag/AgCl, (f) correlative electron micrograph of SECCM area, (g) respective CV for the single particle (highlighted by green dashed circle), and (h) high-resolution electron micrograph. (i) Averaged CV response at individual Au NCs (n = 101) and Au ODs (n = 99). The pixel resolution of the SECCM CV map in (a,e) was 200 nm/pixel for both X and Y axes. Inset: Same averaged CVs without standard deviation errors bars. (j) Histogram of current magnitude at −0.80, −0.90, and −0.95 V vs Ag/AgCl. Data recorded in aqueous 100 mM $HClO_4$, scan rate = 1 V/s.

on a mixture of Au NCs and ODs deposited onto the same glassy carbon substrate (Figure 4). Thirteen individual Au NCs and 27 Au ODs, spanning 20 and 43 pixels, respectively, were identified via correlative SECCM and SEM imaging (Figures S22 and S23). A histogram of current magnitudes at −0.95 V vs Ag/AgCl for isolated Au NCs and Au ODs on the Au mixture samples (Figure S24) showed that higher current was more frequently observed at individual Au NCs compared to Au ODs. This trend is in a good agreement with results presented in Figure 3 when Au NCs and Au ODs were studied on separate substrates. A SECCM CV map and corresponding SEM image for the Au mixture sample acquired at −1.05 V vs Ag/AgCl is shown in Figure 4a,b, where pixels corresponding to three Au NCs, three Au ODs, and two misshaped particles are highlighted by the green circles. The particle morphology was verified by SEM (Figure 4f). CVs corresponding to those eight selected particles show that at −1.05 V vs Ag/AgCl, Au NCs exhibit the highest current among the three types of NPs with lower current assigned to Au ODs and the misshaped particles (Figure 4c−e). A comparison of the electrochemical response and exposed surface area of individual Au NCs and Au ODs in the mixture sample yielded a negligible surface area dependence, at the single-particle level, on the electrochemical response (Figure S25). This suggests that there are other factors that can lead to differences in current response among the Au NCs and Au ODs (i.e., variations in the extent of ligand removal at the interface between the bottom flat facet of the NP and glassy carbon electrode and at facets on the NP in contact with the SECCM droplet). A previous study demonstrated that the molecular adsorption (or linking) characteristics of ligands on Au NPs could also significantly influence the catalytic performance by stabilizing the Au NPs and modifying electronic density and steric state of nanocatalyst structure.[33] Analysis of the Au mixture sample underscores the advantage of correlative SECCM with SEM, over macroscale measurements, to separate the electrochemical responses at misshaped particles from the responses at particles that are correctly faceted.

Data from SECCM studies at faceted Au NPs highlight several factors. First, drop-cast solutions, as opposed to electrocatalytically grown or surfaces with more elaborate preparation strategies, can be used to quantitatively evaluate the electrochemical response of unique, individual electrocatalysts. Second, for studies here, experiments operate in an interesting regime, where the size of the fluid at the tip (estimated diameter 200−400 nm) is comparable to the size of the particles being measured. In this regime, tip (where the tip is the droplet)−sample interactions become increasingly important. To assess the possible impacts of incomplete droplet encapsulation of individual NPs during SECCM acquisition, the voltammetric responses of NC and OD particles (Supporting Information, section S6) as a function

https://dx.doi.org/10.1021/acs.nanolett.9b04640
Nano Lett. 2020, 20, 1233−1239

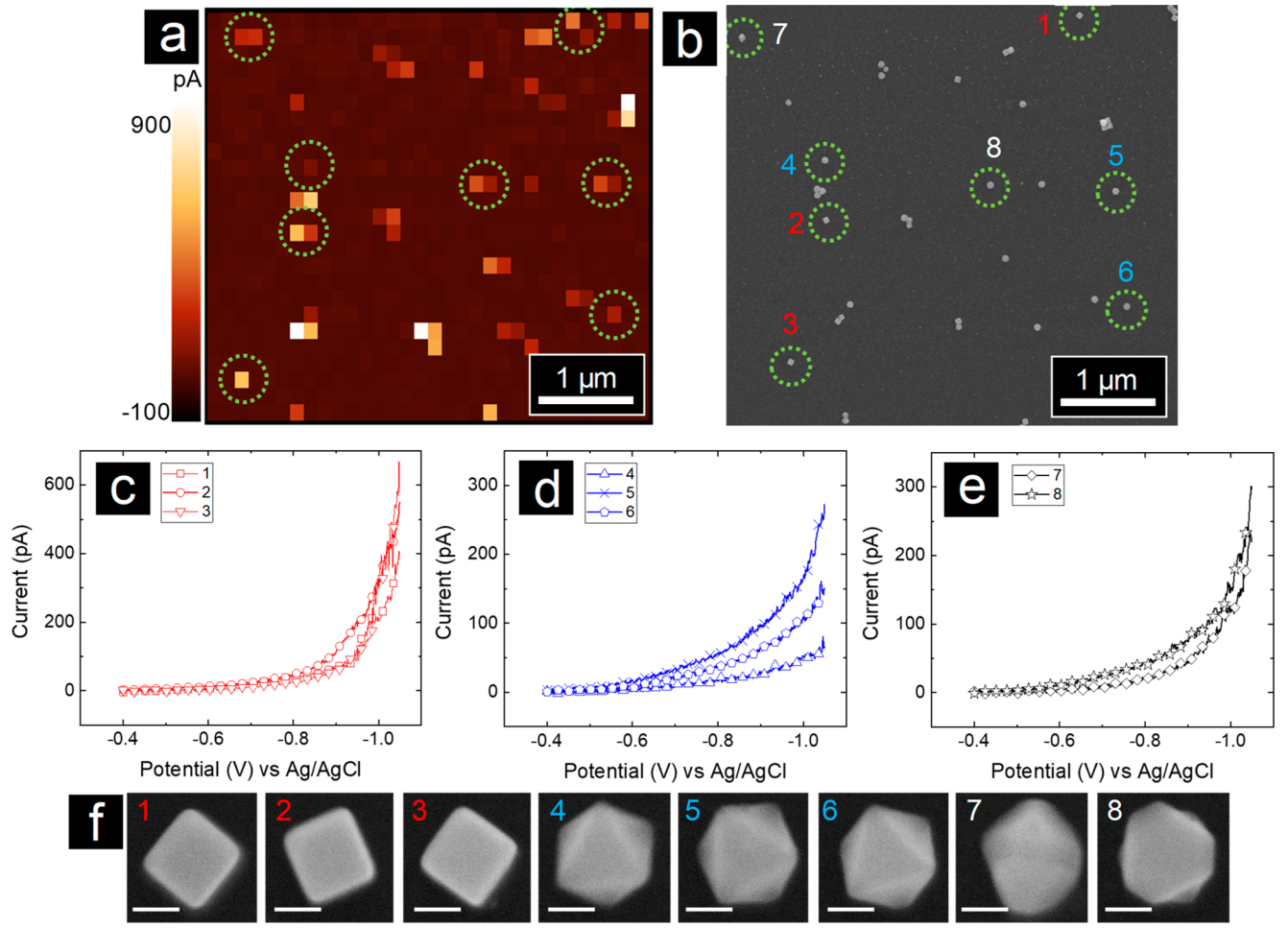

Figure 4. (a) SECCM CV map of a mixture of Au NCs and Au ODs with substrate bias at −1.05 V and (b) correlative electron micrograph of the same area. CVs at individual (c) Au NCs, (d) Au ODs, and (e) misshaped particles. (f) High-resolution electron micrographs of each individual particle (scale bar = 50 nm). Red, blue, and white numbers in (b) and (f) correspond to individual Au NCs, Au ODs, and misshaped particles, respectively. Note, if more than one pixel showed an enhanced current response for an individual particle, only the pixel corresponding to the highest current was included in the CVs. The solution in the pipet was aqueous 100 mM $HClO_4$, scan rate = 1 V/s. The pixel resolution of SECCM CV map in (a) was 200 nm/pixel.

of particle position within the droplet were modeled. These simulations showed no change in $E_{1/2}$ but a change in the limiting current (due to exposed particle area, e.g., Figure S26), although these models do not capture changes in kinetic factors. To compare possible kinetic effects for the HER (acquired at low proton concentration), half-wave potentials measured from experiment (Figures S27 and S28, 11 voltammograms) showed a standard deviation of ±9 mV, with the slope showing slight deviation from ideal behavior (simulation) for the parameters used. For these experiments, particles are randomly distributed in the droplet, which suggests there are minimal kinetic effects on $E_{1/2}$. The average steady-state current at single Au NCs measured experimentally (Figures S27 and S28) was found to agree well with finite element models configured to match experimental dimensions (Figure S29), suggesting that typically an isolated Au NC is encapsulated by the drop during SECCM CV mapping. Under experimental conditions studied here (high H^+ concentration, low current density), reductions monitored are most likely a surface-driven process. An additional nominal concern is the possibility of geometric effects on diffusion at fast scan rates at three-dimensional surfaces. To ameliorate this concern, we verified the geometric differences in electrochemical response between single Au NCs and ODs at sizes studied here by finite element simulations of an individual Au NC and Au OD for the ferro-/ferricyanide redox couple. The simulated electrochemical response showed equal steady-state currents at a single Au NC and Au OD (Figure S30), suggesting that the morphology of NPs does not influence the electrochemical response.

In summary, we demonstrated for the first time, that SECCM CV mapping can be utilized to probe the facet-dependent electrocatalytic activity of individual NPs. As a proof-of-concept, we measured the HER activity from a statistically meaningful set of Au NCs and ODs presenting distinct types of crystal planes on their surfaces. Analysis of CVs collected at individual Au NCs and Au ODs by SECCM revealed that Au NCs are catalytically more active for the HER compared to Au ODs. The same trend was observed in macroscale studies, albeit to a smaller extent likely due to sample inhomogeneity. The advancement of nanoscale CV acquisition by SECCM, over classical macroscale methods, provides new insight into quantifying a nanocrystal's catalytic activity at the single-particle level.

https://dx.doi.org/10.1021/acs.nanolett.9b04640
Nano Lett. 2020, 20, 1233−1239

■ ASSOCIATED CONTENT

Supporting Information

The Supporting Information is available free of charge at https://pubs.acs.org/doi/10.1021/acs.nanolett.9b04640.

Synthesis and experimental details, description of SECCM instrument, additional CV maps and electron micrographs, and finite element modeling (PDF)

■ AUTHOR INFORMATION

Corresponding Authors

Xingchen Ye − *Indiana University, Bloomington, Indiana*; orcid.org/0000-0001-6851-2721; Email: xingye@indiana.edu

Lane A. Baker − *Indiana University, Bloomington, Indiana*; orcid.org/0000-0001-5127-507X; Email: lanbaker@indiana.edu

Other Authors

Myunghoon Choi − *Indiana University, Bloomington, Indiana*

Natasha P. Siepser − *Indiana University, Bloomington, Indiana*

Soojin Jeong − *Indiana University, Bloomington, Indiana*

Yi Wang − *Indiana University, Bloomington, Indiana*

Gargi Jagdale − *Indiana University, Bloomington, Indiana*

Complete contact information is available at: https://pubs.acs.org/10.1021/acs.nanolett.9b04640

Author Contributions

‡M.C., N.P.S., and S.J. contributed equally to this work. M.C. and N.P.S. carried out the SECCM experiments and instrument design. S.J. and Y.W. performed nanoparticle synthesis, SECCM sample preparation, and macroscale electrochemical measurements. G.J. carried out the finite element modeling simulations.

Funding

S.J., Y.W., and X.Y. acknowledge primary support from Indiana University FRSP-SEED program and partial support by the National Science Foundation under award number CHE-1808027. M.C., N.P.S., G.J., and L.A.B. and instrument construction efforts were supported by the National Science Foundation (CMI 1507341 and 1808133) and the National Institutes of Health (5R01NS105888-02).

Notes

The authors declare no competing financial interest.

■ ACKNOWLEDGMENTS

The authors thank Electronic Instrument Services (EIS) at Indiana University for help designing and building custom electronics. The IU Nanoscale Characterization Facility is acknowledged for access to and use of the scanning electron microscope, FIB (acquired through the National Science Foundation MRI program (0923064)). Park Systems is gratefully acknowledged for use of their SICM system. Access to computational facilities at Indiana University is supported in part by Lilly Endowment, Inc., through its support for the Indiana University Pervasive Technology Institute.

■ ABBREVIATIONS

NCs, nanocubes; ODs, nano-octahedra; SECCM, scanning electrochemical cell microscopy; HER, hydrogen evolution reaction; ORR, oxygen reduction reaction; CTAB, cetyltrimethylammonium bromide; CV, cyclic voltammetry; CPC, cetylpyridinium chloride; NPs, nanoparticles; WE, working electrode; AC, alternating current; FTIR, Fourier transform infrared; SEM, scanning electron microscopy; LSV, linear sweep voltammetry; MD, molecular dynamics; SECM, scanning electrochemical microscopy

■ REFERENCES

(1) Chiu, C.-Y.; Li, Y.; Ruan, L.; Ye, X.; Murray, C. B.; Huang, Y. Platinum nanocrystals selectively shaped using facet-specific peptide sequences. *Nat. Chem.* **2011**, *3*, 393−399.

(2) Zhang, Q.; Wang, H. Facet-dependent ccatalytic activities of Au nanoparticles enclosed by high-index facets. *ACS Catal.* **2014**, *4*, 4027−4033.

(3) Zhang, J.; Feng, C.; Deng, Y.; Liu, L.; Wu, Y.; Shen, B.; Zhong, C.; Hu, W. Shape-controlled synthesis of palladium single-crystalline nanoparticles: The effect of HCl oxidative etching and facet-dependent catalytic properties. *Chem. Mater.* **2014**, *26*, 1213−1218.

(4) Wang, Z.; Yang, G.; Zhang, Z.; Jin, M.; Yin, Y. Selectivity on etching: Creation of high-energy facets on copper nanocrystals for CO_2 electrochemical reduction. *ACS Nano* **2016**, *10*, 4559−4564.

(5) Zhu, W.; Michalsky, R.; Metin, Ö.; Lv, H.; Guo, S.; Wright, C. J.; Sun, X.; Peterson, A. A.; Sun, S. Monodisperse Au nanoparticles for selective electrocatalytic reduction of CO_2 to CO. *J. Am. Chem. Soc.* **2013**, *135*, 16833−16836.

(6) Dong, A.; Ye, X.; Chen, J.; Kang, Y.; Gordon, T.; Kikkawa, J. M.; Murray, C. B. A generalized ligand-exchange strategy enabling sequential surface functionalization of colloidal nanocrystals. *J. Am. Chem. Soc.* **2011**, *133*, 998−1006.

(7) Xu, W.; Shen, H.; Liu, G.; Chen, P. Single-molecule kinetics of nanoparticle catalysis. *Nano Res.* **2009**, *2*, 911−922.

(8) Hashmi, A. S. K.; Hutchings, G. J. Gold vatalysis. *Angew. Chem., Int. Ed.* **2006**, *45*, 7896−7936.

(9) Kleijn, S. E. F.; Lai, S. C. S.; Koper, M. T. M.; Unwin, P. R. Electrochemistry of manoparticles. *Angew. Chem., Int. Ed.* **2014**, *53*, 3558−3586.

(10) Baker, L. A. Perspective and prospectus on single-entity electrochemistry. *J. Am. Chem. Soc.* **2018**, *140*, 15549−15559.

(11) Bentley, C. L.; Edmondson, J.; Meloni, G. N.; Perry, D.; Shkirskiy, V.; Unwin, P. R. Nanoscale electrochemical mapping. *Anal. Chem.* **2019**, *91*, 84−108.

(12) Bentley, C. L.; Kang, M.; Unwin, P. R. Scanning electrochemical cell microscopy: New perspectives on electrode processes in action. *Curr. Opin. in Electrochem.* **2017**, *6*, 23−30.

(13) Ebejer, N.; Güell, A. G.; Lai, S. C. S.; McKelvey, K.; Snowden, M. E.; Unwin, P. R. Scanning electrochemical cell microscopy: A versatile technique for nanoscale electrochemistry and functional imaging. *Annu. Rev. Anal. Chem.* **2013**, *6*, 329−351.

(14) Ebejer, N.; Schnippering, M.; Colburn, A. W.; Edwards, M. A.; Unwin, P. R. Localized high resolution electrochemistry and multifunctional imaging: Scanning electrochemical cell microscopy. *Anal. Chem.* **2010**, *82*, 9141−9145.

(15) Snowden, M. E.; Güell, A. G.; Lai, S. C. S.; McKelvey, K.; Ebejer, N.; O'Connell, M. A.; Colburn, A. W.; Unwin, P. R. Scanning electrochemical cell microscopy: Theory and experiment for quantitative high resolution spatially-resolved voltammetry and simultaneous ion-conductance measurements. *Anal. Chem.* **2012**, *84*, 2483−2491.

(16) Dayeh, M.; Ghavidel, M. R. Z.; Mauzeroll, J.; Schougaard, S. B. Micropipette contact method to investigate high-energy cathode materials by using an ionic liquid. *ChemElectroChem* **2019**, *6*, 195−201.

(17) Williams, C. G.; Edwards, M. A.; Colley, A. L.; Macpherson, J. V.; Unwin, P. R. Scanning micropipet contact method for high-resolution imaging of electrode surface redox activity. *Anal. Chem.* **2009**, *81*, 2486−2495.
(18) Saha, P.; Hill, J. W.; Walmsley, J. D.; Hill, C. M. Probing electrocatalysis at individual Au nanorods via correlated optical and electrochemical measurements. *Anal. Chem.* **2018**, *90*, 12832−12839.
(19) Chen, C.-H.; Jacobse, L.; McKelvey, K.; Lai, S. C. S.; Koper, M. T. M.; Unwin, P. R. Voltammetric scanning electrochemical cell microscopy: Dynamic imaging of hydrazine electro-oxidation on platinum electrodes. *Anal. Chem.* **2015**, *87*, 5782−5789.
(20) Liu, D.-Q.; Tao, B.; Ruan, H.-C.; Bentley, C. L.; Unwin, P. R. Metal support effects in electrocatalysis at hexagonal boron nitride. *Chem. Commun.* **2019**, *55*, 628−631.
(21) Tao, B.; Yule, L. C.; Daviddi, E.; Bentley, C. L.; Unwin, P. R. Correlative electrochemical microscopy of Li-ion (de)intercalation at a series of individual $LiMn_2O_4$ particles. *Angew. Chem.* **2019**, *131*, 4654−4659.
(22) Momotenko, D.; Byers, J. C.; McKelvey, K.; Kang, M.; Unwin, P. R. High-speed electrochemical imaging. *ACS Nano* **2015**, *9*, 8942−8952.
(23) Miller, T. S.; Sansuk, S.; E, S. P.; Lai, S. C. S.; Macpherson, J. V.; Unwin, P. R. Pt nanoparticle modified single walled carbon nanotube network electrodes for electrocatalysis: Control of the specific surface area over three orders of magnitude. *Catal. Today* **2015**, *244*, 136−145.
(24) Ustarroz, J.; Ornelas, I. M.; Zhang, G.; Perry, D.; Kang, M.; Bentley, C. L.; Walker, M.; Unwin, P. R. Mobility and poisoning of mass-selected platinum nanoclusters during the oxygen reduction reaction. *ACS Catal.* **2018**, *8*, 6775−6790.
(25) Bentley, C. L.; Kang, M.; Unwin, P. R. Nanoscale structure dynamics within electrocatalytic materials. *J. Am. Chem. Soc.* **2017**, *139*, 16813−16821.
(26) Bentley, C. L.; Unwin, P. R. Nanoscale electrochemical movies and synchronous topographical mapping of electrocatalytic materials. *Faraday Discuss.* **2018**, *210*, 365−379.
(27) Kumatani, A.; Miura, C.; Kuramochi, H.; Ohto, T.; Wakisaka, M.; Nagata, Y.; Ida, H.; Takahashi, Y.; Hu, K.; Jeong, S.; Fujita, J.-i.; Matsue, T.; Ito, Y. Chemical dopants on edge of holey graphene accelerate electrochemical hydrogen evolution reaction. *Adv. Sci.* **2019**, *6*, 1900119.
(28) Takahashi, Y.; Kobayashi, Y.; Wang, Z.; Ito, Y.; Ota, M.; Ida, H.; Kumatani, A.; Miyazawa, K.; Fujita, T.; Shiku, H.; Korchev, Y. E.; Miyata, Y.; Fukuma, T.; Chen, M.; Matsue, T. High resolution electrochemical mapping of hydrogen evolution reaction on transition metal dichalcogenide nanosheets. *Angew. Chem., Int. Ed.* **2019**, DOI: 10.1002/anie.201912863.
(29) Tarnev, T.; Aiyappa, H. B.; Botz, A.; Erichsen, T.; Ernst, A.; Andronescu, C.; Schuhmann, W. Scanning electrochemical cell microscopy investigation of single ZIF-derived nanocomposite particles as wlectrocatalysts for oxygen wvolution in alkaline media. *Angew. Chem., Int. Ed.* **2019**, *58*, 14265−14269.
(30) Novak, P.; Li, C.; Shevchuk, A. I.; Stepanyan, R.; Caldwell, M.; Hughes, S.; Smart, T. G.; Gorelik, J.; Ostanin, V. P.; Lab, M. J.; Moss, G. W. J.; Frolenkov, G. I.; Klenerman, D.; Korchev, Y. E. Nanoscale live-cell imaging using hopping probe ion conductance microscopy. *Nat. Methods* **2009**, *6*, 279.
(31) Ushiki, T.; Nakajima, M.; Choi, M.; Cho, S.-J.; Iwata, F. Scanning ion conductance microscopy for imaging biological samples in liquid: A comparative study with atomic force microscopy and scanning electron microscopy. *Micron* **2012**, *43*, 1390−1398.
(32) Jung, G.-E.; Noh, H.; Shin, Y. K.; Kahng, S.-J.; Baik, K. Y.; Kim, H.-B.; Cho, N.-J.; Cho, S.-J. Closed-loop ARS mode for scanning ion conductance microscopy with improved speed and stability for live cell imaging applications. *Nanoscale* **2015**, *7*, 10989−10997.
(33) Alba-Molina, D.; Puente Santiago, A. R.; Giner-Casares, J. J.; Rodríguez-Castellón, E.; Martín-Romero, M. T.; Camacho, L.; Luque, R.; Cano, M. Tailoring the ORR and HER electrocatalytic performances of gold nanoparticles through metal−ligand interfaces. *J. Mater. Chem. A* **2019**, *7*, 20425−20434.
(34) Meena, S. K.; Celiksoy, S.; Schäfer, P.; Henkel, A.; Sönnichsen, C.; Sulpizi, M. The role of halide ions in the anisotropic growth of gold nanoparticles: a microscopic, atomistic perspective. *Phys. Chem. Chem. Phys.* **2016**, *18*, 13246−13254.
(35) Hamelin, A.; Weaver, M. J. Dependence of the kinetics of proton reduction at gold electrodes on the surface cyrstallographic orientation. *J. Electroanal. Chem. Interfacial Electrochem.* **1987**, *223*, 171−184.
(36) Brug, G. J.; Sluyters-Rehbach, M.; Sluyters, J. H.; Hemelin, A. The kinetics of the reduction of protons at polycrystalline and monocrystalline gold electrodes. *J. Electroanal. Chem. Interfacial Electrochem.* **1984**, *181*, 245−266.
(37) Hamelin, A.; Stoicoviciu, L.; Chang, S.-C.; Weaver, M. J. Temperature dependence of proton electroreduction kinetics at gold(111) and (210) surfaces and annealing of surface defects. *J. Electroanal. Chem. Interfacial Electrochem.* **1991**, *307*, 183−194.
(38) Perez, J.; Gonzalez, E. R.; Villullas, H. M. Hydrogen evolution reaction on gold single-crystal electrodes in acid solutions. *J. Phys. Chem. B* **1998**, *102*, 10931−10935.
(39) Yu, Y.; Gao, Y.; Hu, K.; Blanchard, P.-Y.; Noël, J.-M.; Nareshkumar, T.; Phani, K. L.; Friedman, G.; Gogotsi, Y.; Mirkin, M. V. Electrochemistry and electrocatalysis at single gold nanoparticles attached to carbon nanoelectrodes. *ChemElectroChem* **2015**, *2*, 58−63.
(40) Back, S.; Yeom, M. S.; Jung, Y. Active sites of Au and Ag nanoparticle catalysts for CO_2 electroreduction to CO. *ACS Catal.* **2015**, *5*, 5089−5096.

https://dx.doi.org/10.1021/acs.nanolett.9b04640
Nano Lett. 2020, 20, 1233−1239